



Article

# Performance and Mechanisms of Sulfidated Nanoscale Zero-Valent Iron Materials for Toxic TCE Removal from the Groundwater

Yue Lang <sup>1</sup>, Yanan Yu <sup>2</sup>, Hongtao Zou <sup>1,\*</sup>, Jiexu Ye <sup>2</sup> and Shihan Zhang <sup>2</sup>

<sup>1</sup> College of Land and Environment, Shenyang Agricultural University, Shenyang 110866, China; langyue@sjzu.edu.cn

<sup>2</sup> Key Laboratory of Microbial Technology for Industrial Pollution Control of Zhejiang Province, College of Environment, Zhejiang University of Technology, Hangzhou 310014, China; 1112127014@zjut.edu.cn (Y.Y.); yejiexu@zjut.edu.cn (J.Y.); shihanzhang@zjut.edu.cn (S.Z.)

\* Correspondence: hongtaozou208@126.com

**Abstract:** Trichloroethylene (TCE) is one of the most widely distributed pollutants in groundwater and poses serious risks to the environment and human health. In this study, sulfidated nanoscale zero-valent iron (S-nZVI) materials with different Fe/S molar ratios were synthesized by one-step methods. These materials degraded TCE in groundwater and followed a pathway that did not involve the production of toxic byproducts such as dichloroethenes (DCEs) and vinyl chloride (VC). The effects of sulfur content on TCE dechlorination by S-nZVI were thoroughly investigated in terms of TCE-removal efficiency, H<sub>2</sub> evolution, and reaction rate. X-ray diffraction (XRD) and X-ray Photoelectron Spectroscopy (XPS) characterizations confirmed Fe(0) levels in S-nZVI were larger than for zero-valent iron (nZVI). An Fe/S molar ratio of 10 provided the highest TCE-removal efficiencies. Compared with nZVI, the 24-h TCE removal efficiencies of S-nZVI (Fe/S = 10) increased from 30.2% to 92.6%, and the Fe(0) consumed during a side-reaction of H<sub>2</sub> evolution dropped from 77.0% to 12.8%. This indicated the incorporation of sulfur effectively inhibited H<sub>2</sub> evolution and allowed more Fe(0) to react with TCE. Moreover, the pseudo-first-order kinetic rate constants of S-nZVI materials increased by up to 485% compared to nZVI. In addition, a TCE degradation was proposed based on the variation of detected degradation products. Noting that acetylene, ethylene, and ethane were detected rather than DCEs and VC confirmed that TCE degradation followed  $\beta$ -elimination with acetylene as the intermediate. These results demonstrated that sulfide modification significantly enhanced nZVI performance for TCE degradation, minimized toxic-byproduct formation, and mitigated health risks. This work provides some insight into the remediation of chlorinated-organic-compound-contaminated groundwater and protection from secondary pollution during remediation by adjusting the degradation pathway.

**Keywords:** S-nZVI; sulfidation; trichloroethylene; pathway; groundwater safety



**Citation:** Lang, Y.; Yu, Y.; Zou, H.; Ye, J.; Zhang, S. Performance and Mechanisms of Sulfidated Nanoscale Zero-Valent Iron Materials for Toxic TCE Removal from the Groundwater. *Int. J. Environ. Res. Public Health* **2022**, *19*, 6299. <https://doi.org/10.3390/ijerph19106299>

Academic Editor: Cheng Yan

Received: 10 April 2022

Accepted: 17 May 2022

Published: 22 May 2022

**Publisher's Note:** MDPI stays neutral with regard to jurisdictional claims in published maps and institutional affiliations.



**Copyright:** © 2022 by the authors. Licensee MDPI, Basel, Switzerland. This article is an open access article distributed under the terms and conditions of the Creative Commons Attribution (CC BY) license (<https://creativecommons.org/licenses/by/4.0/>).

## 1. Introduction

Chlorinated hydrocarbons are common industrial solvents. Accidental spills and improper disposal result in these organic compounds entering the soil, drinking water, and groundwater [1–5]. Trichloroethene (TCE) is an intensively detected chlorinated hydrocarbon in groundwater [6,7]. It readily migrates, is persistent in abiotic and biotic degradation, and poses serious threats to groundwater [8–12]. TCE poses a significant carcinogenic risk to human health by all routes of exposure [13] and is classified as “carcinogenic to humans” by the International Agency for Research on Cancer [14]. TCE exposure is associated with kidney cancer, liver cancer, and lymphatic-system cancer. Groundwater serves as a primary source of drinking water in China, which underscores the importance of developing an

environmentally friendly technology to remediate the TCE-contaminated groundwater in order to mitigate its health risks.

Methods such as adsorption, oxidation/reduction, and biologically reductive dechlorination have been used to eliminate TCE in groundwater [2,15,16]. Among these methods, nanoscale zero-valent iron (nZVI) is promising for the in situ chemical remediation of TCE-contaminated groundwater, readily reacting and dechlorinating TCE into non-toxic end products [17]. However, nZVI readily reacts with dissolved oxygen, water, and other groundwater substrates to form iron oxides and/or hydroxides. The continuously thickened iron oxide or hydroxide shell passivates the nZVI surface, which decreases the electron-transfer efficiency between Fe(0) and the pollutants in the inner core, and decreases nZVI activity [18–22]. Furthermore, nZVI shows relatively poor selectivity for TCE reduction over water in an aqueous solution [23].

In response to these problems, many groups have reported their research regarding ZVI modification to improve its reactivity, selectivity, and longevity. A few recent studies have reported that sulfidation could improve nZVI performance in the reduction of chlorinated contaminants. During sulfidation, FeS forms on the nZVI surface, thereby enhancing electron transfer between Fe(0) and chlorinated hydrocarbons and restraining hydrogen ( $H_2$ ) evolution between Fe(0) and water [24–26]. Kim et al. reported that 'Fe/FeS' nanoparticles, synthesized via dithionite addition, enhanced TCE removal as compared to nZVI [27]. Rajajayavel and Ghoshal reported that sulfidation of nZVI facilitated TCE dechlorination and suggested the Fe/S molar ratio played a key role in the reactivity of sulfidated nZVI (S-nZVI) [28]. Han and Yan reported that enhanced TCE dechlorination rates with increasing sulfur levels were only significant at low sulfur loadings, which differed from the findings of Rajajayavel and Ghoshal [23,28]. Thus, although incorporating sulfur into nZVI has been demonstrated, S-nZVI needs additional refinement for better TCE dechlorination, and the critical variables such as sulfur content and speciation need a systematic investigation. Moreover, the abiotic TCE-degradation pathway typically follows one of three pathways such as hydrogenolysis,  $\alpha$ -elimination, and  $\beta$ -elimination [17]. Among them,  $\beta$ -elimination is promising since it produces acetylene as an intermediate rather than highly toxic DCEs and VC [28]. Therefore, in-depth research on the pathway of TCE dechlorination is specifically needed for S-nZVI.

In this study, S-nZVI materials with different Fe/S molar ratios were prepared using sodium dithionite as the sulfidation agent. The effects of Fe/S molar ratios on the morphology and structure were characterized by scanning electron microscopy (SEM), Brunner–Emmet–Teller measurements (BET), X-ray diffraction (XRD), and X-ray photoelectron spectroscopy (XPS). The reactivities of different S-nZVI materials and bare nZVI to TCE and water were assessed with respect to TCE-removal efficiency,  $H_2$  evolution, and the kinetics of TCE degradation. Furthermore, dechlorination products and pathways were identified in order to gain insight into the mechanism of S-nZVI for TCE degradation and the mitigation of health risks. This work provides some guidance to develop green and environmentally friendly technologies to remediate chlorinated-organic-compound-contaminated groundwaters and protect them from secondary pollution and potential health risks.

## 2. Materials and Methods

### 2.1. Reagents

$FeSO_4 \cdot 7H_2O$  (>99%, Analytical Reagent), ethanol (99.8%, Guaranteed Reagent) and NaOH (95%, Analytical Reagent) were purchased from Rhawn (Shanghai, China).  $NaBH_4$  (98%, Analytical Reagent) was purchased from Sinopharm Chemical Reagents Ltd., (Shanghai, China). TCE ( $C_2HCl_3$ , >99.5%, Guaranteed Reagent) and  $Na_2S \cdot 9 H_2O$  (>98.0%, Analytical Reagent) were purchased from Aladdin (Shanghai, China).  $N_2$  (purity 99.99%), air (purity 99.99%), Ar (purity 99.99%) and  $H_2$  (purity 99.99%) were purchased from Hangzhou Jingong Special Gas Co., Ltd. (Hangzhou, China).  $H_2$  standard gas (10%) and

Alkane olefin standard gas (purity 99.99%) were purchased from Dalian Date Gas Co., Ltd. (Dalian, China).

## 2.2. Preparation of nZVI

A total of 4.9643 g of  $\text{FeSO}_4 \cdot 7\text{H}_2\text{O}$  was dissolved in 50 mL deoxygenated water and transferred into a 250 mL three-necked flask. Absolute ethanol (20 mL) was added and stirred to dilute the dispersed solute and make the synthesized iron particles smaller.  $\text{NaBH}_4$  (2.0266 g) (excess  $\text{Fe}^{2+}:\text{BH}_4^- = 1:3$ ) was dissolved in 20 mL of 0.1% NaOH solution (inhibiting  $\text{NaBH}_4$  hydrolysis). The mixture was added dropwise using a constant-pressure funnel to a three-neck flask at 2 drops/s and stirred at 1000 rpm. After the dropwise addition was completed, stirring was continued for 0.5 h. Then, the nZVI particle was separated from the suspension using a magnet, and washed with deoxygenated deionized water and pure ethanol three times. After that, the material was sequentially dried in an argon-filled glove box for 24 h and aged in the transition chamber of the argon-filled glove box for 8 h. Finally, it was sealed and stored in the anaerobic glove box. All the reactant solutions used in the experiment were stripped with  $\text{N}_2$  for at least 0.5 h to remove the dissolved oxygen.

## 2.3. One-Step Preparation of S-nZVI

A total of 3.723 g of  $\text{FeSO}_4 \cdot 7\text{H}_2\text{O}$  was added into 110 mL of deoxygenated water and stirred for 0.5 h under  $\text{N}_2$  atmosphere in a 250 mL three-necked flask. Then, 7.5 mL of aq. NaOH (1 M) was added dropwise into the  $\text{FeSO}_4$  solution at a rate of 1 drop/s while stirring. A total of 1.0165 g of  $\text{NaBH}_4$  was dissolved into 40 mL of deoxygenated water, and a certain amount of 0.1 M  $\text{Na}_2\text{S} \cdot 9\text{H}_2\text{O}$  solution was added in order to prepare a synthesis mixture. After that, the mixture of  $\text{NaBH}_4$  and  $\text{Na}_2\text{S}$  solution were introduced into the three-necked flask at a rate of 0.2 mL/s by a peristaltic pump, followed by 0.5 h of mechanically stirring under an atmosphere of  $\text{N}_2$ . The dosages of  $\text{Na}_2\text{S} \cdot 9\text{H}_2\text{O}$  solution in the synthesis mixture were 52.23, 26.12, 17.41 and 13.06 mL to achieve the Fe/S molar ratios of 2.5, 5, 7.5 and 10, respectively. The resulting S-nZVI suspension was washed at least three times with the deoxygenated deionized water and pure ethanol, and dried in an argon-filled glove box for 24 h. Finally, the obtained S-nZVI particles were placed in the transition chamber of the anaerobic glove box for 8 h of aging, and then sealed and stored in the argon-filled glove box. All the reactant solutions used in the experiment were purged with  $\text{N}_2$  for at least 0.5 h to remove the dissolved oxygen.

## 2.4. TCE Degradation and $\text{H}_2$ Evolution

Inside an anaerobic glove box, 0.026 g of S-nZVI or nZVI was added to a 52 mL crimp-top vial containing 26 mL of a deoxygenated 4-(2-hydroxyethyl)-1-piperazine ethane sulfonic acid (HEPES) buffer (50 mM, pH = 7), and sealed with an aluminum cover and a polytetrafluoroethylene (PTFE) septum. Outside the glove box, 15  $\mu\text{L}$  of a 0.136 M TCE stock solution was injected to ensure an initial TCE concentration of 10 ppm. Finally, the crimp-top vial was placed on a constant-temperature shaker and maintained at 30 °C. At certain intervals, 100  $\mu\text{L}$  of headspace gas in the bottle was extracted with a micro-sampling needle; the TCE concentration,  $\text{H}_2$  concentration, and the TCE-degradation products were measured by GC. The solution pH in the bottle was measured after the reaction.

## 2.5. Characterization

A physical adsorption instrument (Mike 2460 type, Norcross, GA, USA) measured the adsorption isotherm of the material on  $\text{N}_2$  at 77 K using  $\text{N}_2$  as the adsorbate to calculate the specific surface area and pore size of the material. The samples were degassed at 120 °C for 6 h before testing, and the specific BET surface area of the tested material was determined based on the  $\text{N}_2$  adsorption and desorption of BJH models at 77 K. The surface morphology of the material was analyzed by SEM (Zeiss Sigma 300, Oberkochen, Germany). The surface composition of the material was analyzed using XPS (K-AlpHa, Thermo Scientific, Waltham,

MA, USA). The initial binding energy of the XPS spectrum was corrected based on the C1s peak at 284.8 eV, and the energy spectrum was analyzed using XPS-peak fit software (V4.1, USA). The crystal type of the material was qualitatively analyzed by XRD (X'Pert'3 Powder, Panalytical, Almelo, The Netherlands). The test conditions of the instrument were as follows: the X-ray source was Cu target K $\alpha$  rays ( $\lambda = 0.154056$  nm), with a scanning range of 10–80° at a scanning rate of 5° min<sup>-1</sup>.

## 2.6. Kinetic Modelings

The degradation of TCE followed the pseudo-first-order reaction kinetics (Equation (1))

$$y = Ae^{-k_{sa}t} \quad (1)$$

where  $k_{sa}$  (L/(m<sup>2</sup>·h)) refers to the pseudo-first-order reaction-rate constant,  $y$  (mg/L) represents the TCE concentration of headspace sampling in the crimp-top vial,  $t$  (h) represents the reaction time, and  $A$  (mg/L) represents the initial TCE concentration.

## 2.7. Analytical Methods

Concentrations of TCE and its degradation products were measured by a GC (Agilent 7890B, Santa Clara, CA, USA) equipped with a flame ionization detector (FID). The capillary column was a GS-Q, 30 m long with a 0.53 mm diameter. The inlet temperature was 200 °C, the detector temperature was 230 °C, the injection volume was 100  $\mu$ L, and the injection port split ratio was 10:1. The initial column oven temperature was 50 °C, maintained for 7 min, then increased to 230 °C at a heating rate of 20 °C/min for 10 min. During this process, TCE and its degradation products in the samples were separated.

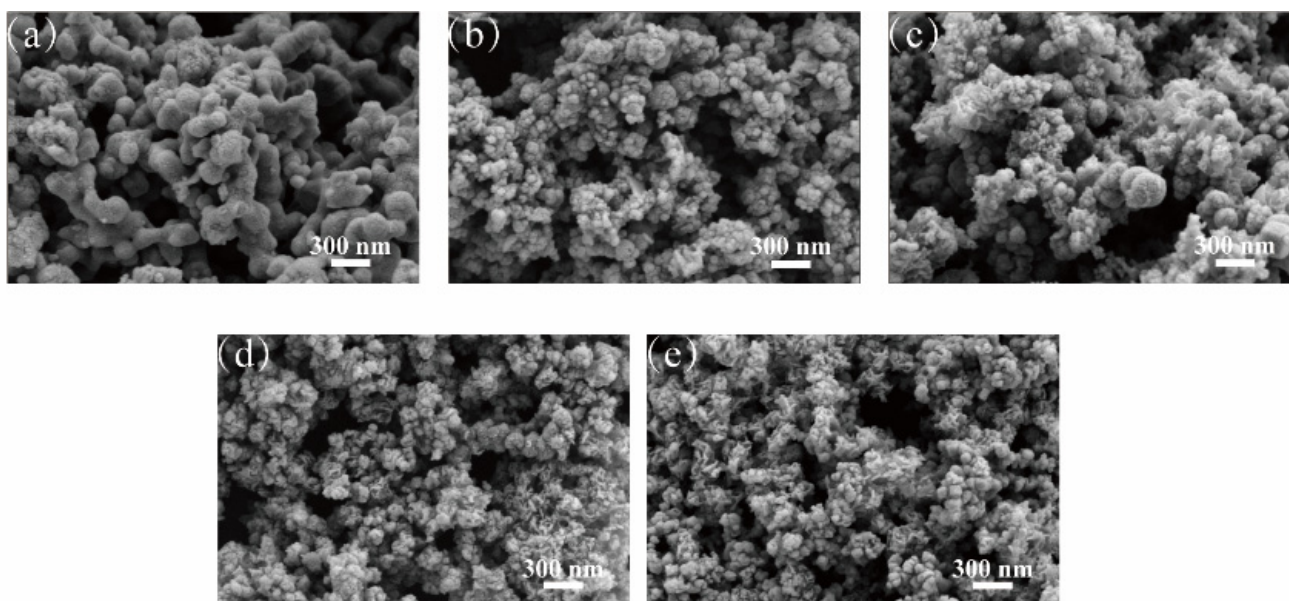
The concentration of H<sub>2</sub> was measured by a gas chromatograph (FULI-9790, Taizhou, China) equipped with a thermal conductive detector (TCD). A TXD-01 packed column (3 mm  $\times$  2 m, Lanzhou Institute of Chemical Physics, Chinese Academy of Sciences, Lanzhou, China) was used, with Ar as the carrier gas. The inlet temperature was 140 °C, the column oven was 60 °C, the detector temperature was 140 °C, and the injection volume was 100  $\mu$ L. Since H<sub>2</sub> solubility in water is negligible, H<sub>2</sub> in the reaction-vial headspace was the total H<sub>2</sub> produced during the reaction.

## 3. Results and Discussion

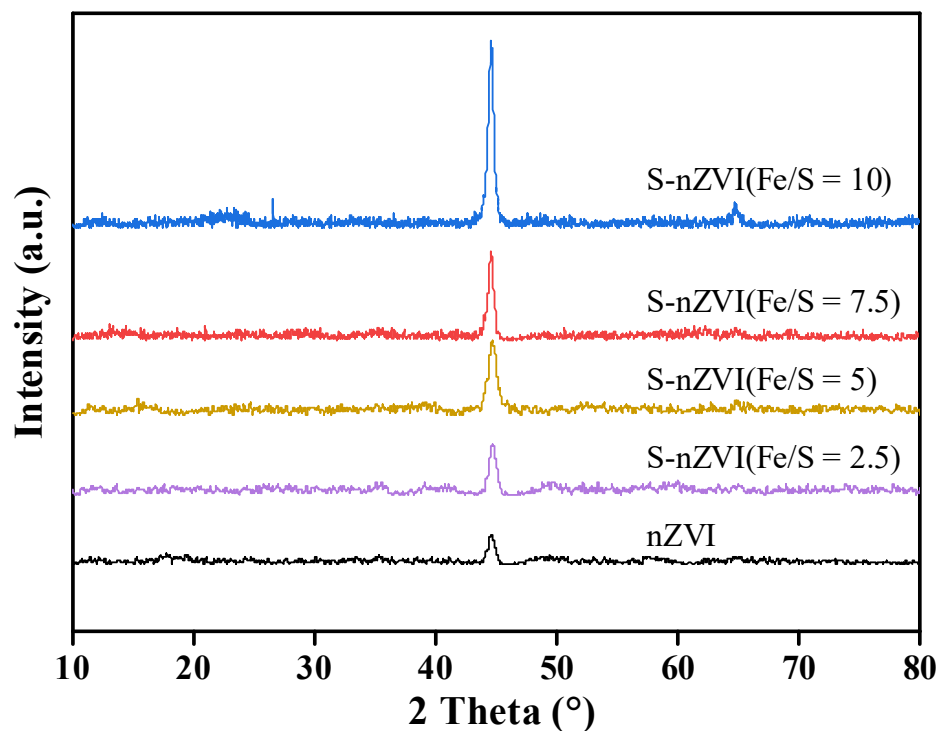
### 3.1. Materials Characterization

Figure 1 shows the surface morphology of nZVI and S-nZVI materials with different Fe/S molar ratios. Figure 1a shows spherical nZVI particles with relatively uniform sizes (50–200 nm) that aggregate into chains due to electrostatic and magnetic forces. The S-nZVI contained spherical and amorphous structures as shown in Figure 1b–e. By comparing S-nZVI materials with different Fe/S ratios, the spherical structure continuously decreased, and the main structure gradually changed from a relatively regular sphere to an irregular amorphous structure as sulfur was added. These changes illustrated that sulfidation increased material dispersion and improved its specific surface area, which could be related to the formation of an FeS<sub>x</sub> layer on the nZVI surface.

Figure 2 shows XRD spectra of nZVI and S-nZVI with different Fe/S ratios. The characteristic diffraction peaks at  $2\theta = 44.6^\circ$  and  $65.0^\circ$  corresponded to the (110) and (200) faces of Fe(0) (PDF#00-006-0696), respectively. On the other hand, there was no obvious iron-oxide peak, which indicated that the degree of oxidation was relatively light during the preparation and preservation of the material. Additionally, S-nZVI had a strong diffraction peak at the same position, which indicated high crystallinity Fe(0) in S-nZVI, and that sulfur introduction promoted the formation of Fe(0) crystals, and the peak intensity increased with the increase of Fe/S ratio.



**Figure 1.** SEM images of nZVI and S-nZVI materials with different Fe/S molar ratios (a) nZVI; (b) S-nZVI (Fe/S = 10); (c) S-nZVI (Fe/S = 7.5); (d) S-nZVI (Fe/S = 5); (e) S-nZVI (Fe/S = 2.5).



**Figure 2.** XRD spectra of nZVI and S-nZVI materials with different Fe/S molar ratios.

The pore structure and size of different materials were analyzed to explore surface-structure differences among nZVI and S-nZVI materials with different Fe/S ratios. As shown in Table 1, the specific surface area of nZVI was  $8.76 \text{ m}^2/\text{g}$ , and the specific surface areas of S-nZVI with different Fe/S ratios (2.5, 5, 7.5, and 10) were 95.66, 53.52, 57.60, and  $27.11 \text{ m}^2/\text{g}$ , respectively. The specific surface area and pore volume increased with added sulfur, perhaps due to the presence of  $\text{FeS}_x$ , which inhibited material agglomeration and increased the surface roughness and surface area. For Fe/S = 5 and 2.5, the average pore size and volume both increased significantly. This might be due to increased  $\text{FeS}_x$ ; the amorphous structure became the primary structure, which resulted in larger pore size

and volume. This conclusion agreed with SEM image data. These results indicated the Fe/S ratio significantly impacted the pore size and characteristics of S-nZVI as well as its reaction activity.

**Table 1.** Pore-structure parameters of nZVI and S-nZVI materials with different Fe/S ratios.

| Sample              | $S_{BET}$ ( $m^2/g$ ) | $D_{average}$ (nm) | $V_{total}$ ( $cm^3/g$ ) |
|---------------------|-----------------------|--------------------|--------------------------|
| nZVI                | 8.76                  | 3.41               | 0.01                     |
| S-nZVI (Fe/S = 10)  | 27.11                 | 3.82               | 0.05                     |
| S-nZVI (Fe/S = 7.5) | 57.60                 | 3.41               | 0.12                     |
| S-nZVI (Fe/S = 5)   | 53.52                 | 22.17              | 0.31                     |
| S-nZVI (Fe/S = 2.5) | 95.66                 | 18.91              | 0.48                     |

XPS analysis determined the elemental composition and valence information on the material surface. Fe 2p peak fitting (Figure 3a) yielded binding energies for Fe 2p 3/2, Fe(III), Fe(II), and Fe(0) at 711.0, 709.0, and 706.7 eV, respectively, while Fe 2p 1/2, Fe(III), Fe(II), and Fe(0) had binding energies of 724.8, 722.8, and 719.8 eV, respectively. Shoulder peaks for Fe(III) and Fe(II) came at 718.9 and 733.4 eV, and 714.6 and 729.5 eV, respectively. Additionally, no obvious elemental-iron peaks were observed because the XPS analysis determined the nanomaterial components on the surface. Fitting data revealed the S-nZVI surface was covered by iron sulfide, so the ZVI content was not detected. As shown in Figure 3c, the one-step sulfidation of nZVI showed a drop in the Fe(III) content with additional sulfur, while levels of Fe(II) remained steady. Peak fitting of S 2p in the material is shown in Figure 3b, in which the binding energies of monosulfide ( $S^{2-}$ ), disulfide ( $S_2^{2-}$ ), and sulfate ( $SO_4^{2-}$ ) were 161.5, 162.2, and 168.5 eV, respectively. As shown in Figure 3d, S in S-nZVI mainly existed as  $S^{2-}$ ,  $S_2^{2-}$ , or  $SO_4^{2-}$ . With added sulfur,  $S^{2-}$  levels decreased, and the content of  $S_2^{2-}$  increased, possibly due to excessive sulfur (from sodium sulfide) that reduced to  $S_2^{2-}$ , and the electron-transfer utilization of  $FeS_2$  was much smaller than  $FeS$  [29], so the generation of excessive  $S_2^{2-}$  reduced its electron-transfer efficiency and reduced dechlorination of S-nZVI on TCE.

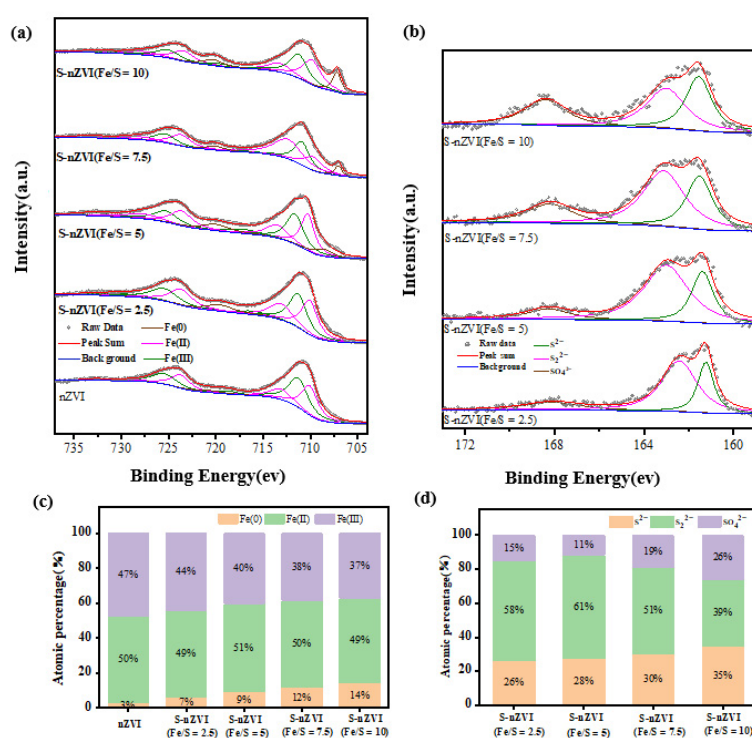


**Figure 3.** XPS spectra of nZVI and S-nZVI materials with different Fe/S ratios: (a) XPS spectrum of Fe 2p; (b) XPS spectrum of S 2p; (c) Fe levels in different valences; (d) S levels in different valences.

### 3.2. Performance of TCE Degradation

Figure 4 shows the performances of nZVI and S-nZVI materials with different Fe/S ratios (Fe/S = 2.5, 5, 7.5, and 10) in TCE degradation. As shown in Figure 4a, the 24 h TCE-removal efficiency of nZVI was 30.2%, while that of S-nZVI (Fe/S = 10) exceeded 92.6%, which indicated that nZVI did not degrade TCE, while the dechlorination of S-nZVI improved significantly. Meanwhile, the removal efficiency of TCE increased as the Fe/S molar ratio increased. To confirm whether Fe (not S) degraded TCE in S-nZVI, Na<sub>2</sub>S was mixed with TCE to monitor its degradation effect. As shown in Figure 4a, Na<sub>2</sub>S did not degrade TCE. A quantitative test of H<sub>2</sub> in the crimp-top vial was performed (Figure 4b) to explore how much Fe(0) was used for H<sub>2</sub> evolution. That test indicated that the side reaction of H<sub>2</sub> evolution consumed 77.0% of the initial Fe(0) in nZVI. However, only 12.8% of the initial Fe(0) was consumed for H<sub>2</sub> evolution in the S-nZVI at an Fe/S ratio of 10. This indicated that sulfidation greatly inhibited side reactions so that a large amount of Fe(0) could react fully with TCE. Some researchers reported that H<sub>2</sub> evolution mainly occurred in the iron oxide layer rather than the FeS<sub>x</sub> layer, while the main reaction site for TCE occurred in the FeS<sub>x</sub> layer [30,31]. Since the FeS<sub>x</sub> layer had strong electrical conductivity [32], electron transfer from the surface of the FeS<sub>x</sub> layer was used for TCE degradation. This was the reason S-nZVI simultaneously suppressed H<sub>2</sub> evolution and promoted TCE degradation.

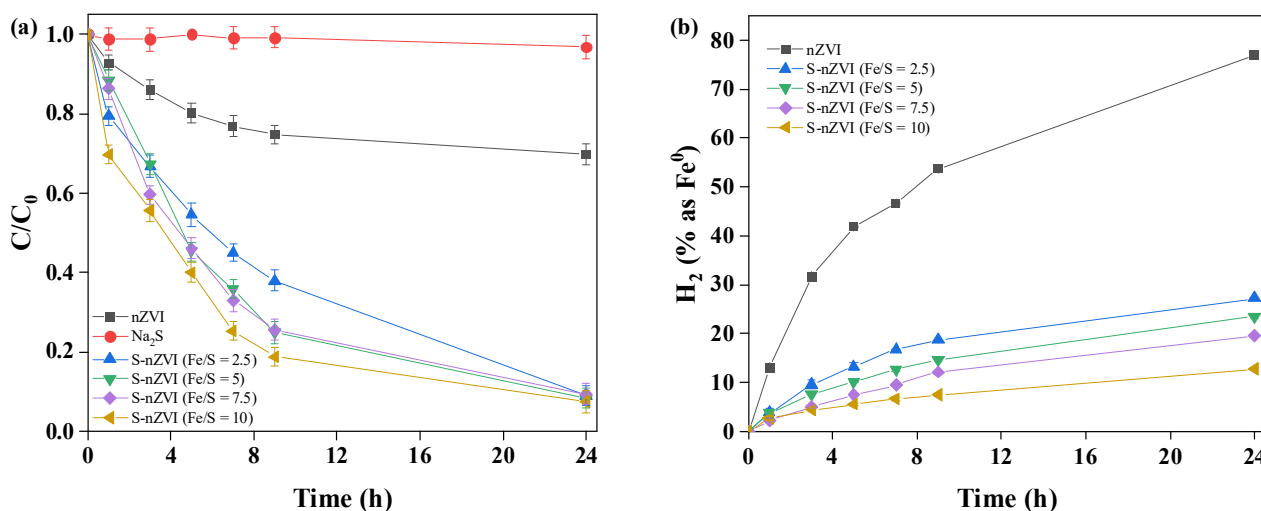


**Figure 4.** Performance of nZVI and S-nZVI materials with different Fe/S molar ratios in TCE degradation, (a) TCE removal; (b) H<sub>2</sub> evolution (pH: 7, t: 30 °C; S-nZVI: 0.026 g, TCE: 10 ppm).

### 3.3. Kinetics of TCE Degradation

An evaluation of degradation rate constants for nZVI and S-nZVI materials was conducted and is shown in Figure 5. Rate constants were obtained by fitting the 24 h removal-efficiency curve for TCE using pseudo-first-order kinetics. As shown in Figure 5, the incorporation of sulfur into nZVI greatly increased the degradation rate constant, which was likely due to the FeS shell of S-nZVI improving electron-transfer efficiency. The degradation activity of S-nZVI maximized for Fe/S = 10, with a rate constant of 0.117 L/(m<sup>2</sup>·h). However, when the Fe/S molar ratio varied between 2.5–10, the rate constant for S-nZVI materials changed slightly. This may be related to excess Fe(0) in the S-nZVI system, where the initial TCE concentration was as low as 10 ppm.

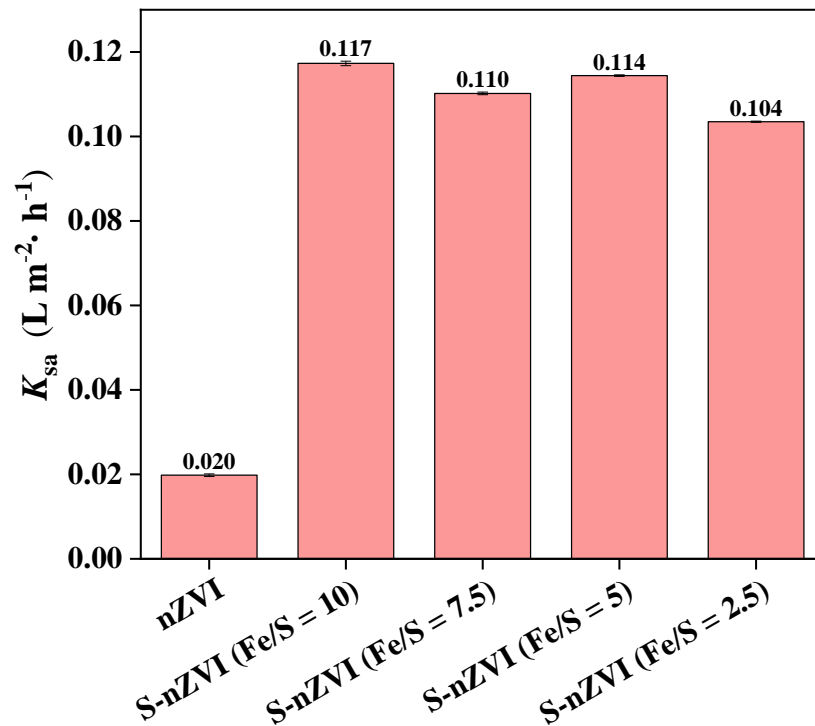


**Figure 5.** Reaction rates of TCE degradation by nZVI and S-nZVI materials with different Fe/S molar ratios. (pH: 7, t: 30 °C; nZVI and S-nZVI: 0.026 g, TCE: 10 ppm).

### 3.4. Mechanism of TCE Degradation

As shown in Figure 6, toxic products such as DCEs and VC were not detected in either neat nZVI or S-nZVI. Moreover, both materials primarily produced ethylene, which confirmed that TCE degradation followed a  $\beta$ -elimination mechanistic pathway with acetylene as the intermediate. In this work, primary products of TCE degradation such as acetylene, ethylene, and ethane were measured and are shown in Figure 6. Compared with the neat nZVI, a small amount of acetylene was detected with the S-nZVI, which indicated that sulfidated modification of nZVI enhanced the conversion of TEC to form acetylene. Moreover, the ethylene produced using S-nZVI was 11.3 times greater than nZVI, which confirmed that sulfidated modification enhanced the reactivity of each step during TCE degradation.

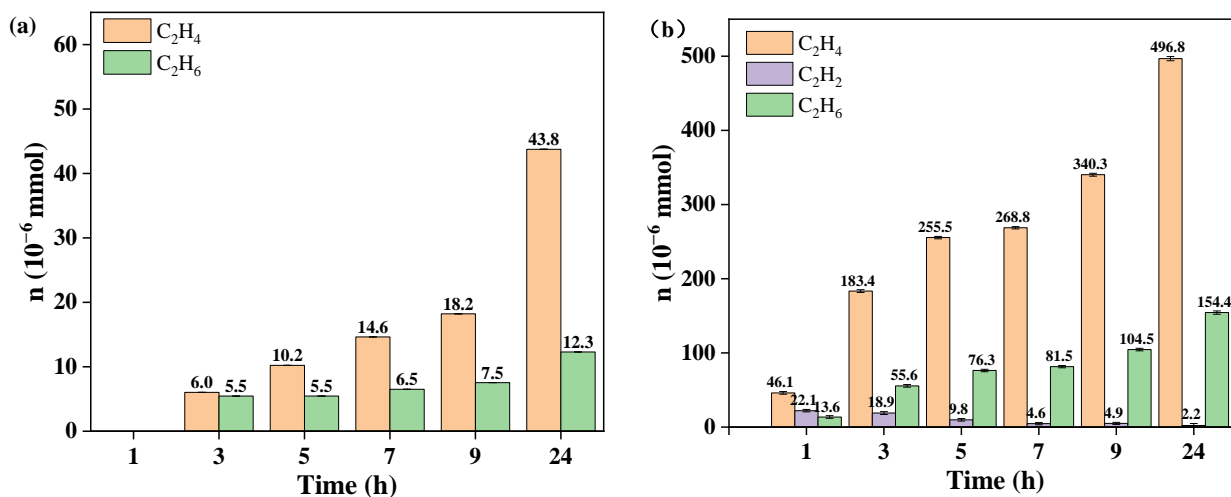


**Figure 6.** Gas phase production during TCE degradation with: (a) neat nZVI; and (b) S-nZVI with a Fe/S ratio of 10 (pH: 7, T: 30 °C; nZVI and S-nZVI: 0.026 g).

Overall, dechlorination of TCE occurred via  $\beta$ -elimination through chloroacetylene, followed by hydrogenolysis of chloroacetylene to acetylene, which agreed with previous reports [23,33]. A larger dose of S-nZVI produced ethylene and ethane via hydrogenation of acetylene, and may generate C<sub>3</sub>–C<sub>6</sub> hydrocarbons via the polymerization of acetylene (Figure 7).

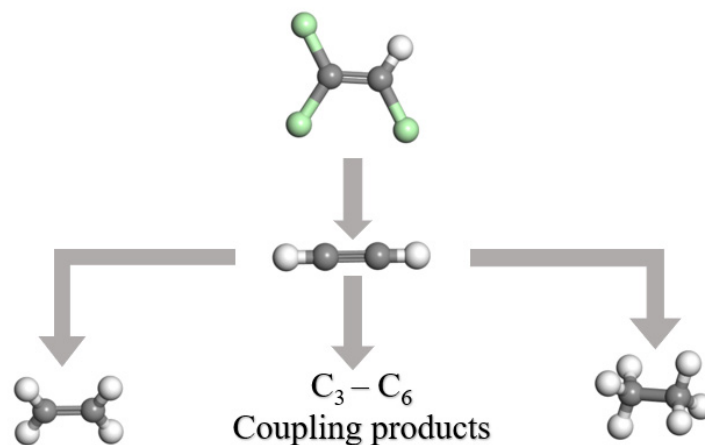


**Figure 7.** A possible mechanism for the TCE degradation with the S-nZVI.

#### 4. Conclusions

This study found that sulfidation significantly improved TCE dechlorination via nZVI. XRD and XPS results illustrated that sulfidation caused the material to store more Fe(0), and Fe(0) increased with the decreasing sulfur ratio ( $\text{Fe}/\text{S} \leq 10$ ). The 24 h TCE-removal efficiency of S-nZVI with an Fe/S ratio of 10 increased from 30.2% to 92.6% compared to nZVI. This was attributed to a reduction in H<sub>2</sub> evolution from nZVI after sulfidation. At an Fe/S molar ratio of 10, Fe(0) consumed by H<sub>2</sub> evolution was only 12.8%, which suggested a large amount of reactive Fe(0) was available to react with TCE. Compared with nZVI, the pseudo-first-order kinetic rate constants of S-nZVI materials increased significantly. Additionally, the reaction of TCE degradation by S-nZVI was explored. Acetylene was the intermediate product, followed by the production of ethylene and ethane. C<sub>3</sub>–C<sub>6</sub> hydrocarbons may be generated via the polymerization of acetylene. Overall, this work provides insights into developing green and environmentally friendly technologies to remediate chlorinated organic compound-contaminated groundwater and protect them from secondary pollution as well as potential health risks in groundwater utilization.

**Author Contributions:** Y.L.: Writing—Original Draft, Investigation; Y.Y.: Investigation, Data Analysis. H.Z.: Conceptualization, Supervision, Validation; J.Y.: Formal Analysis; S.Z.: Writing—Review & Editing. All authors have read and agreed to the published version of the manuscript.

**Funding:** This work was supported by the Central Government Guided Local Science and Technology Development Fund (2021ZY1022), and National Natural Science Foundation of China (Nos: 21876157).

**Institutional Review Board Statement:** Not applicable.

**Informed Consent Statement:** Not applicable.

**Data Availability Statement:** The data presented in this study are available on request from the corresponding author. The data are not publicly available due to privacy.

**Conflicts of Interest:** The authors declare no conflict of interest.

## References

1. Seyama, T.; Adachi, K.; Yamazaki, S. Kinetics of photocatalytic degradation of trichloroethylene in aqueous colloidal solutions of TiO<sub>2</sub> and WO<sub>3</sub> nanoparticles. *J. Photochem. Photobiol. A* **2012**, *249*, 15–20. [[CrossRef](#)]
2. Wei, Z.S.; Seo, Y. Trichloroethylene (TCE) adsorption using sustainable organic mulch. *J. Hazard. Mater.* **2010**, *181*, 147–153. [[CrossRef](#)] [[PubMed](#)]
3. Dong, H.R.; He, Q.; Zeng, G.M.; Tang, L.; Zhang, L.H.; Xie, Y.K.; Zeng, Y.L.; Zhao, F. Degradation of trichloroethene by nanoscale zero-valent iron (nZVI) and nZVI activated persulfate in the absence and presence of EDTA. *Chem. Eng. J.* **2017**, *316*, 410–418. [[CrossRef](#)]
4. Huang, B.B.; Lei, C.; Wei, C.H.; Zeng, G.M. Chlorinated volatile organic compounds (Cl-VOCs) in environment-sources, potential human health impacts, and current remediation technologies. *Environ. Int.* **2014**, *71*, 118–138. [[CrossRef](#)] [[PubMed](#)]
5. Valentin, L.; Nousiainen, A.; Mikkonen, A. Introduction to Organic Contaminants in Soil: Concepts and Risks. In *Emerging Organic Contaminants in Sludges: Analysis, Fate and Biological Treatment*; Springer: Berlin/Heidelberg, Germany, 2013; pp. 1–29. [[CrossRef](#)]
6. Yan, J.C.; Han, L.; Gao, W.G.; Xue, S.; Chen, M.F. Biochar supported nanoscale zerovalent iron composite used as persulfate activator for removing trichloroethylene. *Bioresour. Technol.* **2015**, *175*, 269–274. [[CrossRef](#)]
7. Dong, H.R.; Zhang, C.; Deng, J.M.; Jiang, Z.; Zhang, L.H.; Cheng, Y.J.; Hou, K.J.; Tang, L.; Zeng, G.M. Factors influencing degradation of trichloroethylene by sulfide-modified nanoscale zero-valent iron in aqueous solution. *Water Res.* **2018**, *135*, 1–10. [[CrossRef](#)]
8. Dong, H.R.; Zhang, C.; Hou, K.J.; Cheng, Y.J.; Deng, J.M.; Jiang, Z.; Tang, L.; Zeng, G.M. Removal of trichloroethylene by biochar supported nanoscale zero-valent iron in aqueous solution. *Sep. Purif. Technol.* **2017**, *188*, 188–196. [[CrossRef](#)]
9. Starr, R.C.; Orr, B.R.; Lee, M.H.; Delwiche, M. *Final Project Report-Coupled Biogeochemical Process Evaluation for Con-Ceptualizing Trichloroethylene Co-Metabolism: Co-Metabolic Enzyme Activity Probes and Modeling Co-Metabolism and Attenuation*; North Wind Inc.: Idaho Falls, ID, USA, 2010.
10. Slater, G.F.; Dempster, H.S.; Sherwood Lollar, B.; Ahad, J. Headspace analysis: A new application for isotopic characterization of dissolved organic contaminants. *Environ. Sci. Technol.* **1999**, *33*, 190–194. [[CrossRef](#)]
11. Meng, Q.J.; Li, P.F.; Qu, J.H.; Liu, Y.; Wang, Y.F.; Chen, Z.B.; Zhang, Y. Study on the community structure and function of anaerobic granular sludge under trichloroethylene stress. *Ecotoxicology* **2021**, *30*, 1408–1418. [[CrossRef](#)]
12. Chiu, W.A.; Jinot, J.; Scott, C.S.; Makris, S.L.; Cooper, G.S.; Dzubow, R.C.; Bale, A.S.; Evans, M.V.; Guyton, K.Z.; Keshava, N.; et al. Human health effects of trichloroethylene: Key findings and scientific issues. *Environ. Health Persp.* **2013**, *121*, 303–311. [[CrossRef](#)]
13. Luo, Y.-S.; Furuya, S.; Soldatov, V.Y.; Kosyk, O.; Yoo, H.S.; Fukushima, H.; Lewis, L.; Iwata, Y.; Rusyn, I. Metabolism and Toxicity of Trichloroethylene and Tetrachloroethylene in Cytochrome P450 2E1 Knockout and Humanized Transgenic Mice. *Toxicol. Sci.* **2018**, *164*, 489–500. [[CrossRef](#)]
14. Guha, N.; Loomis, D.; Grosse, Y.; Lauby-Secretan, B.; El Ghissassi, F.E.; Bouvard, V.; Benbrahim-Tallaa, L.; Baan, R.; Mattock, H.; Straif, K. Carcinogenicity of trichloroethylene, tetrachloroethylene, some other chlorinated solvents, and their metabolites. *Lancet Oncol.* **2012**, *13*, 1192–1193. [[CrossRef](#)]
15. Ahmad, M.; Lee, S.S.; Dou, X.M.; Mohan, D.; Sung, J.-K.; Yang, J.E.; Ok, Y.S. Effects of pyrolysis temperature on soybean stover- and peanut shell-derived biochar properties and TCE adsorption in water. *Bioresour. Technol.* **2012**, *118*, 536–544. [[CrossRef](#)] [[PubMed](#)]
16. Shao, H.B.; Butler, E.C. The Relative Importance of Abiotic and Biotic Transformation of Carbon Tetrachloride in Anaerobic Soils and Sediments. *Soil Sediment. Contam. Int. J.* **2009**, *18*, 455–469. [[CrossRef](#)]
17. Pasinszki, T.; Krebsz, M. Synthesis and Application of Zero-Valent Iron Nanoparticles in Water Treatment, Environmental Remediation, Catalysis, and Their Biological Effects. *Nanomaterials* **2020**, *10*, 917. [[CrossRef](#)]
18. Mu, Y.; Jia, F.L.; Ai, Z.H.; Zhang, L.Z. Iron oxide shell mediated environmental remediation properties of nano zero-valent iron. *Environ. Sci. Nano* **2017**, *4*, 27–45. [[CrossRef](#)]
19. Zhang, W.-X. Nanoscale Iron Particles for Environmental Remediation: An Overview. *J. Nanoparticle Res.* **2003**, *5*, 323–332. [[CrossRef](#)]
20. Nurmi, J.T.; Tratnyek, P.G.; Sarathy, V.; Baer, D.R. Characterization and properties of metallic iron nanoparticles: Spectroscopy, electrochemistry, and kinetics. *Environ. Sci. Technol.* **2005**, *39*, 1221–1230. [[CrossRef](#)]
21. Fan, D.M.; Anitori, R.P.; Tebo, B.M.; Tratnyek, P.G.; Lezama Pacheco, J.S.; Kukkadapu, R.K.; Engelhard, M.H.; Bowden, M.E.; Kovarik, L.; Arey, B.W. Reductive sequestration of pertechnetate (99TcO<sub>4</sub><sup>-</sup>) by nano zerovalent iron (nZVI) trans-formed by abiotic sulfide. *Environ. Sci. Technol.* **2013**, *47*, 5302–5310. [[CrossRef](#)]
22. Park, S.W.; Kim, S.K.; Kim, J.B.; Choi, S.W.; Inyang, H.I.; Tokunaga, S. Particle surface hydrophobicity and the dechlorination of chloro-compounds by iron sulfides. *Water Air Soil Pollut.* **2006**, *6*, 97–110. [[CrossRef](#)]
23. Han, Y.L.; Yan, W.L. Reductive dechlorination of trichloroethene by zero-valent iron nanoparticles: Reactivity enhancement through sulfidation treatment. *Environ. Sci. Technol.* **2016**, *50*, 12992–13001. [[CrossRef](#)] [[PubMed](#)]
24. Fan, D.; Lan, Y.; Tratnyek, P.G.; Johnson, R.L.; Filip, J.; O'Carroll, D.M.; Garcia, A.N.; Agrawal, A. Sulfidation of Iron-Based Materials: A Review of Processes and Implications for Water Treatment and Remediation. *Environ. Sci. Technol.* **2017**, *51*, 13070–13085. [[CrossRef](#)] [[PubMed](#)]

25. Li, J.X.; Zhang, X.Y.; Sun, Y.K.; Liang, L.P.; Pan, B.C.; Zhang, W.M.; Guan, X.H. Advances in Sulfidation of Zerovalent Iron for Water Decontamination. *Environ. Sci. Technol.* **2017**, *51*, 13533–13544. [[CrossRef](#)] [[PubMed](#)]
26. Garcia, A.N.; Zhang, Y.Y.; Ghoshal, S.; He, F.; O'Carroll, D.M. Recent advances in sulfidated zerovalent iron for contaminant transformation. *Environ. Sci. Technol.* **2021**, *55*, 8464–8483. [[CrossRef](#)]
27. Kim, E.J.; Kim, J.H.; Azad, A.M.; Chang, Y.S. Facile synthesis and characterization of Fe/FeS nanoparticles for environmental applications. *ACS Appl. Mater. Interfaces* **2011**, *3*, 1457–1462. [[CrossRef](#)]
28. Rajajayavel, S.R.C.; Ghoshal, S. Enhanced reductive dechlorination of trichloroethylene by sulfidated nanoscale zerovalent iron. *Water Res.* **2015**, *78*, 144–153. [[CrossRef](#)]
29. Fang, H.Y.; Huang, T.Z.; Mao, J.F.; Dinesh, M.M.; Sun, Y.; Liang, D.; Qi, L.; Yu, J.M.; Jiang, Z.K. Investigation on the catalytic performance of reduced-graphene-oxide-interpolated FeS<sub>2</sub> and FeS for oxygen reduction reaction. *ChemistrySelect* **2018**, *3*, 10418–10427. [[CrossRef](#)]
30. Mangayayam, M.; Dideriksen, K.; Ceccato, M.; Tobler, D.J. The Structure of Sulfidized Zero-Valent Iron by One-Pot Synthesis: Impact on Contaminant Selectivity and Long-Term Performance. *Environ. Sci. Technol.* **2019**, *53*, 4389–4396. [[CrossRef](#)]
31. Cao, Z.; Liu, X.; Xu, J.; Zhang, J.; Yang, Y.; Zhou, J.L.; Xu, X.H.; Lowry, G.V. Removal of Antibiotic Florfenicol by Sulfide-Modified Nanoscale Zero-Valent Iron. *Environ. Sci. Technol.* **2017**, *51*, 11269–11277. [[CrossRef](#)]
32. Guo, Y.N.; Park, T.; Yi, J.W.; Henzie, J.; Kim, J.; Wang, Z.L.; Jiang, B.; Bando, Y.; Sugahara, Y.; Tang, J.; et al. Nanoarchitectonics for transition-metal-sulfide-based electrocatalysts for water splitting. *Adv. Mater.* **2019**, *31*, 1807134. [[CrossRef](#)]
33. Gu, Y.W.; Wang, B.B.; He, F.; Bradley, M.J.; Tratnyek, P.G. Mechanochemically Sulfidated Microscale Zero Valent Iron: Pathways, Kinetics, Mechanism, and Efficiency of Trichloroethylene Dechlorination. *Environ. Sci. Technol.* **2017**, *51*, 12653–12662. [[CrossRef](#)] [[PubMed](#)]